Nonlinear Processes in Geophysics (2002) 9: 1–10

Nonlinear Processes in Geophysics

Numerical simulations of a three-wave coupling occurring in the ionospheric plasma

H. Usui[1], **H. Matsumoto**[1], **and R. Gendrin**[1,2]

[1]Radio Science Center for Space and Atmosphere, Kyoto Univerisity Uji, Kyoto 611-0011, Japan
[2]Present address Institut Pierre Simon Laplace, Paris University, 4 Place Jussieu, 75252 Paris, France

Received: 6 November 2000 – Accepted: 20 March 2001

Abstract. We studied a three-wave coupling process occurring in an active experiment of microwave power transmission (MPT) in the ionospheric plasma by performing one-dimensional electromagnetic PIC (Particle-In-Cell) simulations. In order to examine the spatial variation of the coupling process, we continuously emitted intense electromagnetic waves from an antenna located at a simulation boundary. In the three-wave coupling, a low-frequency electrostatic wave is excited as the result of a nonlinear interaction between the forward propagating pump wave and backscattered wave. In the simulations, low-frequency electrostatic bursts are discontinuously observed in space. The discontinuity of the electrostatic bursts is accounted for by the local electron heating due to the bursts and the associated modification of the wave dispersion relation. In a case where the pump wave propagates along the geomagnetic field $\boldsymbol{B}_{ext}$, several bursts of Langmuir waves are observed. Since the first burst consumes a part of the pump wave energy, the pump wave is weakened and cannot trigger the three-wave coupling beyond the region where the burst occurs. Since the dispersion relation of the Langmuir wave is variable, due to the local electron heating by the burst, the coupling condition eventually becomes unsatisfied and the first interaction becomes weak. Another burst of Langmuir waves is observed at a different region beyond the location of the first burst. In the case of perpendicular propagation, the upper hybrid wave, one of the mode branches of the electron cyclotron harmonic waves, is excited. Since the dispersion relation of the upper hybrid wave is less sensitive to the electron temperature, the coupling condition is not easily violated by the temperature increase. As a result, the three-wave coupling periodically takes place in time and eventually, the transmission ratio of the microwaves becomes approximately 20%, while almost no attenuation of the pump waves is observed after the first electrostatic burst in the parallel case. We also examined the dependency of the temporal growth rate for the electrostatic waves on the amplitude of the pump wave.

Correspondence to: H. Usui (usui@kurasc.kyoto-u.ac.jp)

1 Introduction

The idea of transmitting power over long distances by microwaves is rather old. In the Solar Power Satellite (SPS) project, solar energy is collected by a large number of solar cells attached to the satellite and transmitted to a ground station or to another satellite (Glaser, 1968). At the Radio Science Center for Space and Atmosphere of Kyoto University, a program was started in the 80's to study the feasibility and the implications of this concept. Two rocket experiments were conducted in order to study the microwave power transmission (MPT) in the ionosphere: the MINIX experiment (Kaya et al., 1986; Matsumoto and Kimura, 1987) and the METS experiment (Kaya et al., 1993). Both experiments showed that electrostatic waves were excited around the local plasma frequency in association with the microwave emission. In the previous studies of ionospheric heating by HF radio waves, plasma wave excitation was also observed (e.g. Carlson and Duncan, 1977). The associated density modification of electrons and the self-focusing of radio waves were also studied (Duncan and Behnke, 1978; Perkins and Goldman, 1980).

In parallel, theoretical and numerical studies were engaged to evaluate the impact of intense microwaves on space plasmas (Matsumoto, 1982; Matsumoto et al., 1995; Nishikawa, 1999). These studies revealed that the electrostatic wave generation was due to the stimulated Raman scattering type of the three-wave coupling process. It was also found that electrons are heated by the excited electrostatic field. In this process, three waves are basically involved (e.g. Fejer, 1979): an intense electromagnetic wave which plays the role of a pump wave, a backscattered electromagnetic wave with a frequency slightly lower than the frequency of the pump wave, and an electrostatic wave with a frequency much lower than the other two waves.

Meanwhile, an active MPT experiment is proposed by using the JEM (Japan Experimental Module) exposed facility

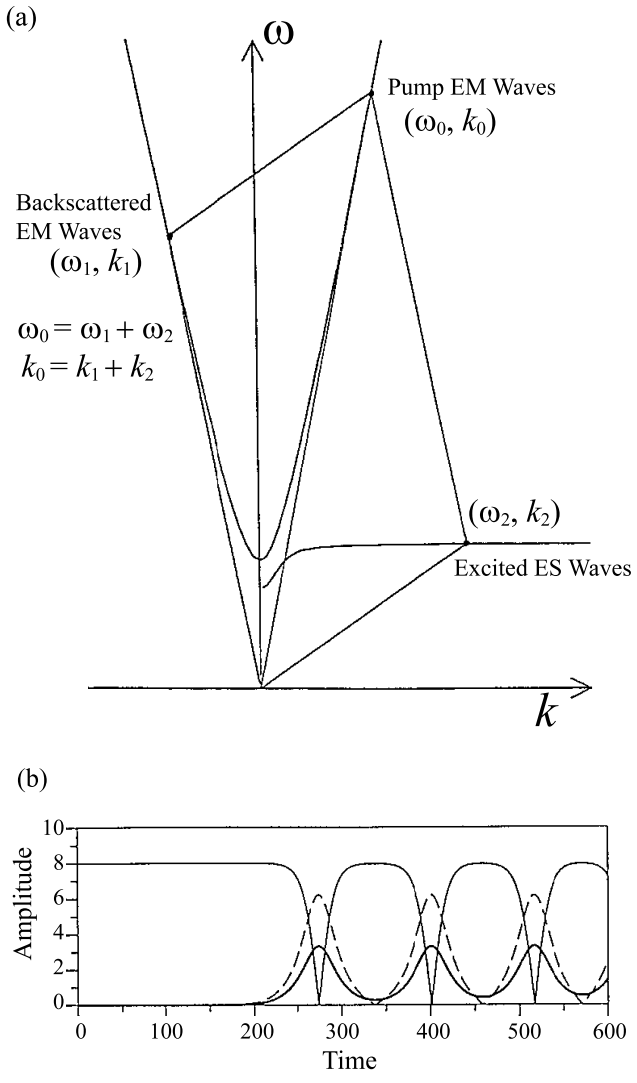

Fig. 1. (a) Schematic illustration of the three-wave coupling process in a $\omega - k$ diagram. For a case in which the wave propagation is perpendicular to $\boldsymbol{B}_{ext}$. The electromagnetic wave can be either ordinary or extraordinary, depending on the relative orientation of the electric field with respect to the external magnetic field $\boldsymbol{B}_{ext}$. The excited electrostatic wave can be one of the mode branches of an electron cyclotron harmonic wave, after Matsumoto et al. (1995). **(b)** Time evolution of a three-wave coupling process: Continuous thin line is the electromagnetic pump wave. Dashed line is the electromagnetic backscattered wave. Bold line is the electrostatic excited wave.

in the International Space Station. The objectives are to test the MPT in space plasma both technically and scientifically with a long-term exposed facility. In particular, by changing the microwave intensity and the angle with respect to the geomagnetic field $\boldsymbol{B}_{ext}$, we will study the possibility of the three-wave coupling process which affects the efficiency of the energy transmission through the space plasma. In the experiments, intense microwaves around several hundred V/m are emitted from an 18 × 18 array antenna as pump waves. The emitted waves are received by another antenna located approximately 2.5 m away from the array antenna. The pump waves are spatially focused by the phase control of the array antenna. Although the experiment has not been approved yet, we performed electromagnetic PIC (Particle-In-Cell) simulations prior to the experiment. In the simulations, we place a microwave antenna at one edge of the simulation system and emit pump waves in one direction. This model enables us to analyze the interaction process not only temporally, but also spatially. In this study, we present a brief review of the three-wave coupling in Sect. 2. In Sects. 3 and 4, we will describe the model and the results of the simulations. In Sect. 5, we will summarize our findings and discuss some of the important physical processes observed in the simulations.

2 Three-wave coupling

Figure 1a shows a schematic illustration of the three-wave coupling process in the $\omega - k$ domain for a case in which the wave propagation is perpendicular to the external magnetic field $\boldsymbol{B}_{ext}$, where ω and k denote frequency and wavenumber, respectively. A pump wave whose frequency and wavenumber are ω_0 and k_0, respectively, causes the backscattered wave with ω_1 and k_1 and the electrostatic wave with ω_2 and k_2.

In the coupling process, the total energy and momentum of the associated waves should be conserved: $\omega_0 = \omega_1 + \omega_2$ and $k_0 = k_1 + k_2$ should be satisfied, respectively. In the MPT in the ionospheric plasma, the pump wave corresponds to intense microwaves emitted from the antenna at a frequency of GHz. The backscattered wave also has a frequency of GHz. These waves can either be ordinary or extraordinary, depending on the relative orientation of its electric field with respect to $\boldsymbol{B}_{ext}$. The excited electrostatic wave can be one of the mode branches of an electron cyclotron harmonic wave. In the case of parallel propagation, the electrostatic wave can be the Langmuir wave.

So far the temporal evolution of the three wave-coupling has been well studied and it can be described with the following mode-coupling equations:

$$\begin{aligned} \frac{dE_0}{dt} &= i\beta_0 E_1 E_2 \\ \frac{dE_1}{dt} &= i\beta_1 E_0 E_2^* \\ \frac{dE_2}{dt} &= i\beta_2 E_0 E_1^* \end{aligned} \tag{1}$$

where E_0, E_1 and E_2 denote the amplitudes of the pump, backscattered, and excited waves, respectively. Quantities with $*$ denote the corresponding complex conjugates. β_0, β_1 and β_2 are the coupling coefficients between the three waves, respectively. $\beta_0 = \beta_1 + \beta_2$ should be satisfied. A schematic illustration of the temporal evolution of each wave amplitude is shown in Fig. 1b. Provided that the amplitude of the pump wave is intense enough, the three-wave coupling process is stimulated and the initial amplitude of the pump wave starts

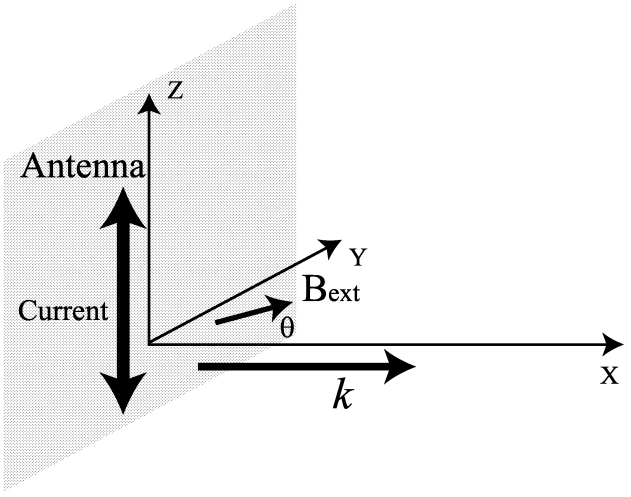

Fig. 2. Geometry of the simulation experiment in the 1-D case. The pump wave is emitted at the origin of the system by a current J_z injected by an antenna. The angle between $\boldsymbol{B}_{ext}$ and the propagation vector can be changed.

to decrease as time elapses. Two waves, the backscattered and excited ones, simultaneously start to grow by satisfying the set of Eq. (1). When the amplitude of the pump wave becomes low enough, the process is reversed. Consequently, the pump wave is no longer absorbed and it can grow in time, until the whole process repeats itself in accordance with the equations.

In the set of Eq. (1), however, no plasma kinetic effects, such as electron heating, is considered. In a real situation, the excited electrostatic waves can heat electrons and may affect the local plasma condition. Therefore, in the present study, we will particularly examine the relation between the excited electrostatic waves and associated electron heating in the coupling process by performing PIC simulations.

3 PIC simulations

3.1 Model

The one-dimensional simulation model adopted in the present study is shown in Fig. 2.

Instead of setting a pump wave uniformly in the system as an initial condition, we emit electromagnetic waves into a magnetized plasma toward the x direction by the continuous oscillation of a current source located at one side of the simulation boundary. In order to see the dependence of the coupling process on the angle with respect to $\boldsymbol{B}_{ext}$, the $\boldsymbol{B}_{ext}$ orientation is variable in the simulations. In a real experiment, we utilize a frequency of the order of 2 GHz for the pump wave, while the plasma frequency of the ionospheric plasma and the electron cyclotron frequency are both in the MHz frequency range. In the present computer experiments, however, we reduce the frequency ratio between the pump wave and the plasma characteristic waves to shorten the computational time. We set the ratios of the plasma frequency and the frequency of the pump wave to the electron cyclotron frequency as 4.0 and 13.2, respectively. Other parameters of the simulation are given in Table 1.

Table 1. Parameters used in the simulations

Plasma parameters		
Sped of light	C_v	100
Electron plasma frequency	ω_p	4.0
Electron cyclotron frequency	Ω_e	-1.0
External magnetic field	$\boldsymbol{B}_{ext}$	1.0
System parameters		
Time step width	Δt	0.01
Unit grid length	Δx	1.0
Number of grids	Nx	1024
Electrons		
Ratio between charge and mass	q/m	-1.0
Number of super particles	Np	32768
Thermal velocity	v_{th}	1.0
Pump electromagnetic wave		
Excitation frequency	ω_0	13.2
Wavenumber (number of modes)	k_0	0.132 (21.5)
Intensity of radiated electric field	$E_0/\lvert\boldsymbol{B}_{ext}C_v\rvert$	2.5

3.2 $\omega - k$ diagram

Figure 3 shows a $\omega - k$ diagram obtained by the Fourier transformation of electromagnetic (EM) and electrostatic (ES) field data in space and time for the parallel propagation case. We analyzed the data for $0 < X\Omega_e/C_v < 10.24$ in space and $0 < \Omega_e t < 20.48$ in time. Note that wave spectra for the pump, backscattered, and electrostatic waves are superimposed in the same $\omega - k$ diagram: the pump wave and the backscattered wave are plotted in the frequency domain above $\omega/\Omega_e = 8$ and the electrostatic wave is plotted in the lower frequency region. The spectra for the pump, backscattered, and electrostatic waves are respectively normalized to their maximum value: $E_{max}/\boldsymbol{B}_{ext}C_v = 112$, 14, and 3. The normalized spectra are plotted for each wavenumber to fit the interval of the horizontal scale. For reference, we imposed dashed lines which correspond to the speed of light, C_v.

It is found that a fraction of the pump wave with (ω_0, k_0) is backscattered with (ω_1, k_1) and then a low-frequency ES wave with (ω_2, k_2) is excited around the local plasma frequency ω_p. Since $\boldsymbol{B}_{ext}$ is along the simulation system, the excited ES waves correspond to the Langmuir mode. As each wave component can be connected with each line of a parallelogram, it is basically confirmed that all three waves satisfy

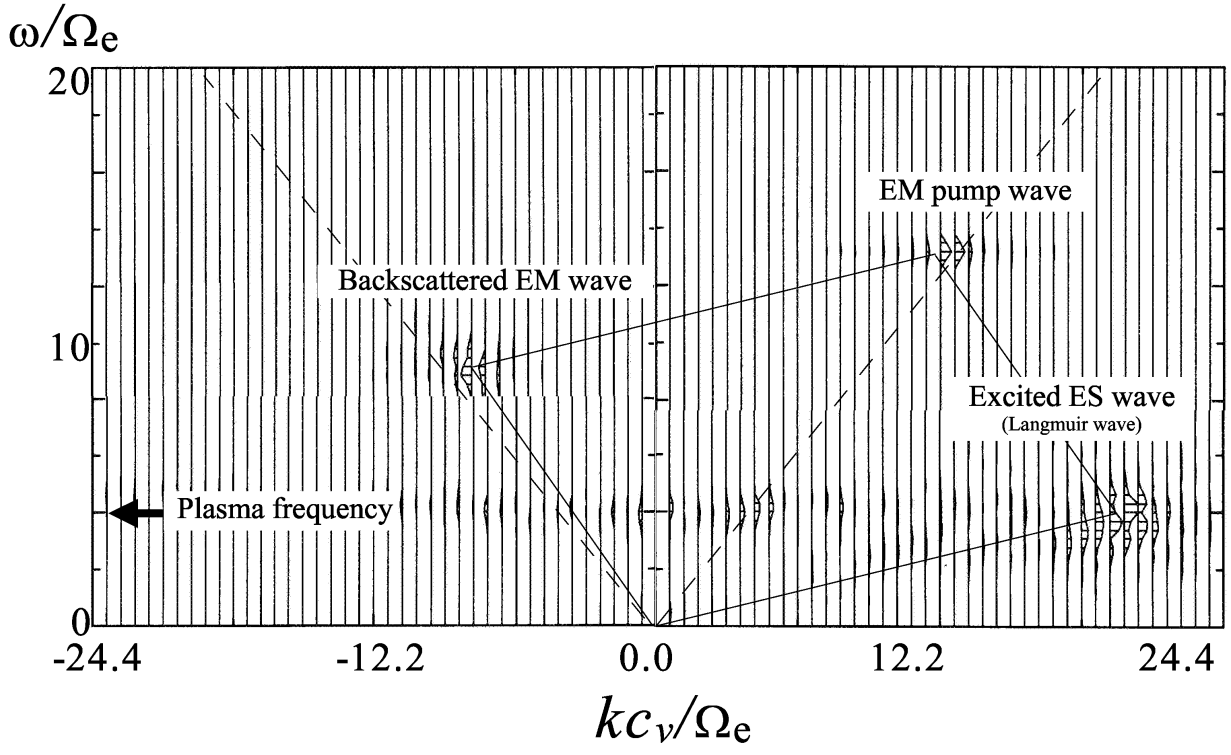

Fig. 3. $\omega - k$ diagram obtained by the Fourier transformation of E_z electromagnetic and E_x electrostatic data in space and time for the parallel case. The obtained wave spectra are plotted at each wavenumber, normalized to their maximum value. The dashed lines correspond to the speed of light. The wavenumber of the most intense electrostatic wave corresponds approximately to $kC_v/\Omega_e \sim 20$.

the relations of the three-wave coupling, as stated in the previous section. One notices an electrostatic component which is excited at smaller wavenumbers with a frequency ω_p. This component is found on the dashed line, which implies that the propagation velocity is C_v. We will discuss the generation of this fast-propagating electrostatic component in the later section.

3.3 Spatial and temporal variation of fields

Figure 4 shows spatial and temporal profiles for EM waves, including the pump or backscattered components, excited ES waves, and the electron temperature in the parallel propagation case. The vertical and horizontal axes show the normalized time and the distance from the antenna location, respectively. In panel (a), we see the pump waves propagating away from the antenna, which is shown as oblique lines originated from the antenna position. The gradient of the lines corresponds to the inverse of C_v. One notices that the field intensity is not constant approximately after $\Omega_e t \sim 10$. Although not clearly shown, there seems to be two regions which have distinct stripes with a large gradient within $X\Omega_e/C_v = 5$: one is found within $X\Omega_e/C_v \sim 2$ around $\Omega_e t \sim 15$, and the other is originated around $X\Omega_e/C_v \sim 5$ and $\Omega_e t \sim 16$, propagating in the backward direction. The stripes are due to the interference between the forward and backward propagating EM waves. Another region with the same stripes is faintly seen after $\Omega_e t \sim 20$ at the further location. In the spatial region approximately between $X\Omega_e/C_v = 5.12$ and 10.24, the amplitude is weak, particularly around $\Omega_e t = 20.48$ to 25.6. This decrease of pump wave amplitude is caused by the energy transfer of the pump wave to the other wave modes in the three-wave coupling process.

In panel (b), as clearly shown around $\Omega_e t = 10.24-20.48$, there are three main bursts of electrostatic waves: one is found near the antenna position approximately after $\Omega_e t = 10$, and the other is at a further region around $\Omega_e t = 15$. The third interaction can be found around $X\Omega_e/c \sim 8$ after $\Omega_e t \sim 20$. These bursts correspond to the regions where the pump wave energy is modified with profiles of large gradient stripes, as stated in the previous paragraph. The profile shows oblique lines which have a much larger gradient than the one corresponding to the EM propagation. This implies that the phase velocity of the intense ES bursts is much smaller than C_v, approximately $0.2\,C_v$. A detailed analysis of panel (b) shows that the ES frequency is of the order of the plasma frequency and that the normalized wavenumber is of the order of 20; both values are confirmed by the Fourier spectrum shown in Fig. 3. Following the intense bursts with a coherent pattern of propagation, a complicated incoherent ES field structure appears in panel (b), particularly after $\Omega_e t \sim 20$. As shown in panel (a), due to the presence of the backscattered pump waves, it may be possible that the backscattered

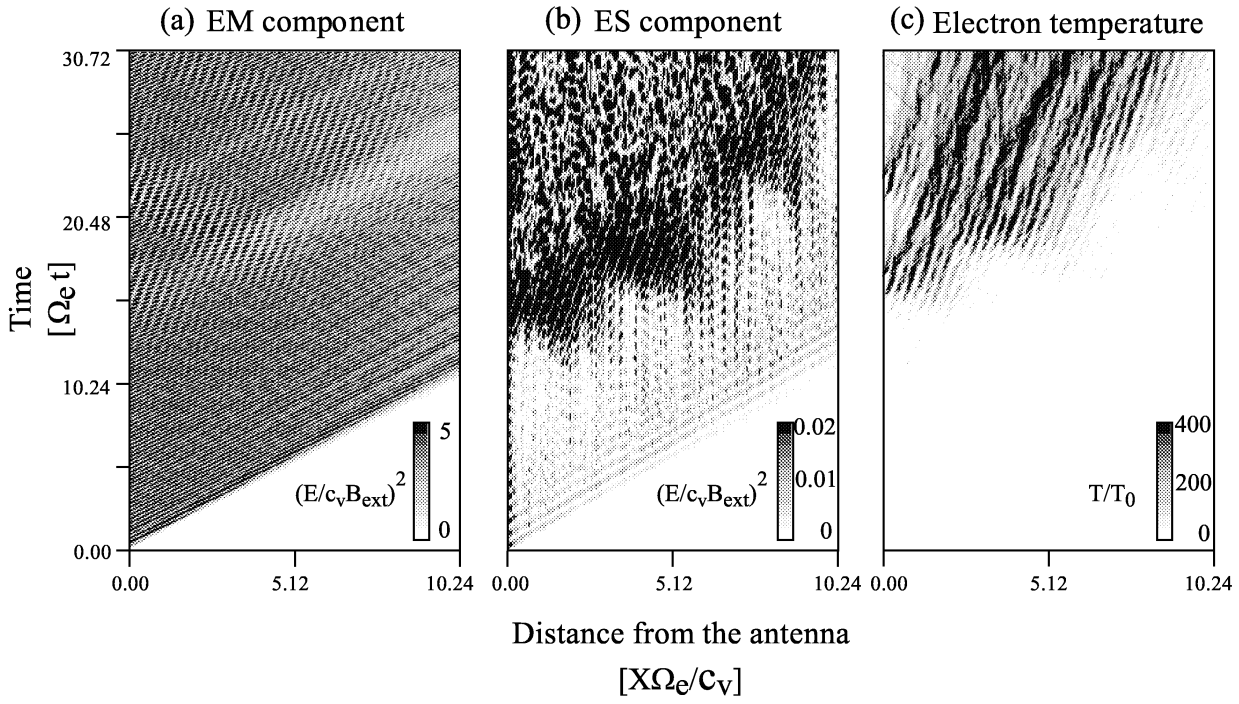

Fig. 4. Evolution of the wave field and of the electron temperature as a function of time and distance. From left to right: EM pump wave energy (E_z), excited ES wave energy (E_x), electron temperature (T_e). In this simulation run, the pump wave intensity $E_0/|\boldsymbol{B}_{ext}C_v|$ is equal to 2.5.

EM wave becomes a pump wave for another three-wave coupling and excites ES waves in the backward direction. Then the forward and backward propagating ES waves cause a standing-like wave, which can cause the complicated incoherent profiles of an ES field. One notices small-amplitude components propagating from the beginning of the simulation run and corresponding to the propagation of EM waves with C_v, as shown in panel (a). This component is also shown in the previous $\omega - k$ diagram at a low wavenumber around ω_p. We will discuss the generation process of this ES component later.

In panel (c), we plot the electron heating in terms of temperature. In accordance with the excitation of the ES waves, the electron temperature increases. Oblique lines in the panel implies that the heated region propagates with the same velocity as the ES field bursts. Considering $\boldsymbol{B}_{ext}$ is in parallel to the simulation system, electrons are resonantly heated and trapped by the excited ES waves and move along $\boldsymbol{B}_{ext}$ with the wave propagation.

In conclusion, in the coupling process, we could observe the excitation of intense ES waves and the associated electron heating. The interesting point we should stress is that the interaction takes places intermittently in space as well as in time. Although we continuously emit the pump wave with constant intensity, the three-wave coupling does not occur continuously in space. This spatial discontinuity of the three-wave coupling process is not described with the Eq. (1) which only express the temporal variations. In a later section, we will discuss in detail the spatial evolution of the coupling process in terms of the ES wave excitation and the associated electron heating.

3.4 Dependence of ES waves on the pump wave intensity

We examined the dependence of the growth of ES waves on the intensity of the pump waves. From the mode-coupling Eq. (1), we can obtain the temporal growth rate of the ES waves $\gamma = \sqrt{|\beta_1\beta_2|}E_0$ on the assumption that dE_0/dt is negligible at the initial stage in comparison with the temporal variation of the other two waves. One notices that γ is proportional to the intensity of the pump waves E_0. To confirm this relation, we performed the computer experiments with different amplitudes of the pump waves: $E_0/|\boldsymbol{B}_{ext}C_v| =$ 1.25, 1.67, 2.5, and 3.75. Time evolutions of the field energy of E_x for each case are superimposed in panel (a) of Fig. 5. As described in the previous section, ES waves are excited in all the cases due to the three-wave coupling. It is found that the excitation occurs more quickly for the case with the larger amplitude of the pump waves. This relation qualitatively agrees with the temporal growth rate stated earlier. To analyze the ES wave excitation quantitatively, we define the temporal growth rate γ for each case from the slope of data in the figure in the time interval where the wave energy grows exponentially. We plot the obtained growth rates normalized to the electron cyclotron frequency in panel (b) of Fig. 5 for $E_0/|\boldsymbol{B}_{ext}C_v| = 1.25$, 1.67, and 2.5. The growth

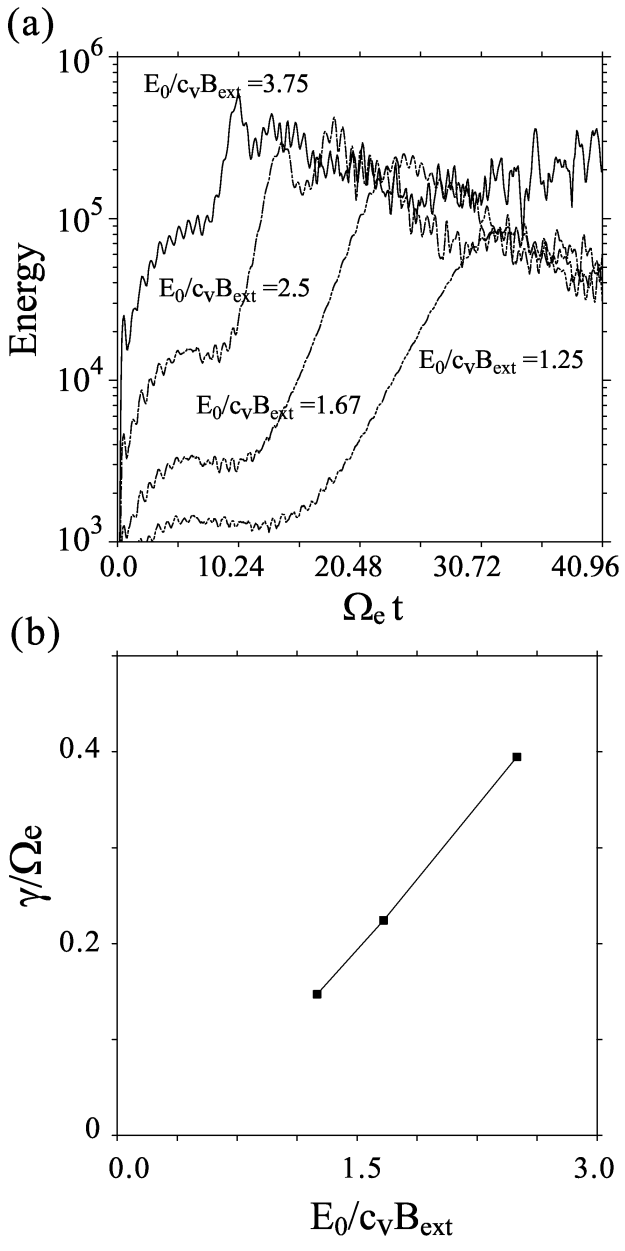

Fig. 5. Relationship between the starting time of the three-wave coupling process and the amplitude of the pump wave. Panel (a) shows the time evolutions of the energy of ES waves excited in the three-wave coupling process with different amplitudes of the pump wave. Panel (b) shows the temporal growth rates for $E_0/|\boldsymbol{B}_{ext}C_v| = 1.25$, 1.67, and 2.5 obtained from the slope of data in panel (a) in a time interval where the wave energy grows exponentially.

rate for the case of $E_0/|\boldsymbol{B}_{ext}C_v| = 3.75$ is not shown in the panel because it is rather difficult to evaluate the value due to the short time interval for the exponential growing phase. We see that the results are almost aligned on one line, which implies that the growth rate γ is proportional to the amplitude of the pump wave E_0.

4 Discussion

4.1 Detail analysis of ES field and electron heating

Figure 6 indicates a detailed analysis of the ES wave excitation and the associated electron heating. The panels focus on the first and second electrostatic bursts. The first burst occurs around $\Omega_e t \sim 10$. The interesting feature we notice is that the region of the ES wave excitation is found up to $X\Omega_e/C_v \sim 3$ from the antenna location and no waves are excited beyond this region until $\Omega_e t \sim 15$. This situation can be interpreted as follows: once the three-wave coupling occurs, a part of the pump waves are backscattered and the forward propagating waves are weakened at the interaction region. Beyond $X\Omega_e/C_v \sim 3$, as shown in Fig. 6, the ES waves are less excited because the pump waves are weakened and cannot trigger the coupling. Corresponding to the ES wave excitation around $X\Omega_e/C_v \sim 3$, electrons are locally heated, as shown in panel (b). In the parallel case, the ES wave is the Langmuir mode whose dispersion relation depends on the electron temperature. As the local temperature increases due to the electron heating, the dispersion relation is modified and does not satisfy the condition of the three-wave coupling. In such a situation, the interaction becomes weak. Correspondingly, the electrons which are resonantly heated by the excited waves propagate away and then the increase of the electron temperature stops around $\Omega_e t \sim 17$. The second three-wave coupling is now ready to occur because the pump waves are less backscattered and can propagate through the system because the first interaction is weakened. Although some of the heated electrons propagate away with the excited ES waves from the region where the first interaction took place, the plasma condition is somewhat modified. Therefore, the second coupling process occurs at a region around $X\Omega_e/C_v = 3 \sim 6$, which is beyond the region for the first interaction. As mentioned earlier, the excited ES waves propagate with the phase velocity of the Langmuir waves.

To see the detail of the electron dynamics, we show phase diagrams of electrons in Fig. 7 at different times: $\Omega_e t = 14.08$, 16.64 and 19.20. In all panels, we see electrons resonantly heated by the excited ES waves. In panel (a), electrons located at the region $0 < X\Omega_e/C_v < 2$ where the first interaction takes place are trapped by the excited ES waves. It is obviously shown that the electron trapping causes the scattering of electrons in the velocity space and the electron temperature increases. In panel (b) which shows the transient phase between the first and second interactions, the electron velocity starts to be modified at the further region $2 < X\Omega_e/C_v$ by the second interaction. In panel (c), the interaction region is shifted to the further location approximately $2.5 < X\Omega_e/C_v < 7.5$ where the second interaction occurs. One notices that most of the electrons near the antenna region are already heated so that the dispersion relation for the Langmuir mode has been modified.

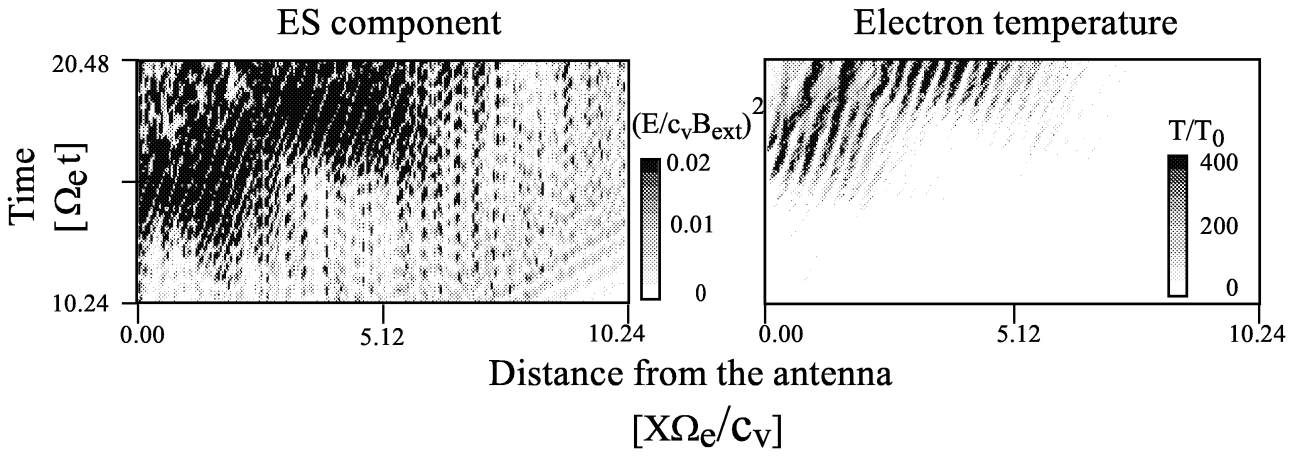

Fig. 6. Successive emissions of ES waves in the case of $\theta = 0$. The left and right panels show the excited ES waves and electron temperature, respectively. The first emission takes place around $\Omega_e t \sim 11$ and $X\Omega_e/C_v \sim 2$. Consequently, electrons are heated and the three-wave matching condition is no longer satisfied. Then the plasma cools and a new interaction can occur around $\Omega_e t \sim 15.5$. and $X\Omega_e/C_v \sim 6$. The pump wave intensity $E_0/|\boldsymbol{B}_{ext}C_v|$ is equal to 2.5.

4.2 Perpendicular case

We examined a case where $\boldsymbol{B}_{ext}$ is along the y direction which is perpendicular to both the directions of the pump wave propagation and the current oscillation of the antenna. Figure 8 shows the profiles of the ES component and the associated electron temperature in the same manner as in Fig. 4. Panel (a) shows that the three-wave coupling occurs intermittently, not continuously in space, as described in the parallel case. We find two main bursts of field excitation around $\Omega_e t \sim 12$ and 16. Unlike the parallel case, the third interaction is hardly seen in the profile. At the antenna region, we also observe an intense ES perturbation which is not directly associated with the three-wave coupling process. We will discuss this generation in a later section. At the later time after the second interaction, the ES field is intensified and the profiles becomes incoherent.

In the perpendicular case, the wave modes which are responsible for the coupling process are either ordinary or extraordinary mode for the EM component and one of the wave branches in the electron cyclotron harmonic (ECH) waves for the ES one. Although not displayed, the Fourier analysis shows that the ES waves are excited near the upper hybrid resonance (UHR) frequency which is very close to the plasma frequency in the present plasma parameters. Namely, the UHR branch in the ECH waves is responsible for the present three-wave coupling.

A big difference from the parallel case is found in panel (b) for the electron temperature. Corresponding to the first and second interactions, electrons are heated by the excited ES waves, which is similar to the parallel case. However, the heating rate is much larger than that in the parallel case: the electrons are heated with almost no delay in the ES wave excitation around $\Omega_e t \sim 12$ and 16 for the first and second interactions, respectively. After the first and second interactions, unlike the parallel case, heated electrons do not propagate away from the antenna region. The electron heating continues at a fixed region $0 < X\Omega_e/C_v < 6$. Moreover, according to the linear dispersion analysis, it is shown that the UHR branch of the ECH waves, unlike the Langmuir wave, is less affected by the variation of the electron temperature (see Matsumoto et al., 1995, Fig. 7). As a result, the condition required for the three-wave coupling is not easily violated by the electron heating and the interaction periodically takes place in the manner as previously shown in the time variation of the three-wave coupling in Fig. 1. As a result, electrons near the antenna region are continuously heated.

4.3 Time variation of the pump wave energy

Figure 9 shows the transmission ratio of the pump wave energy detected at the end of the simulation system ($X\Omega_e/C_v = 10.24$) as a function of time. Solid and dashed lines indicate the energy variations for the cases where $\boldsymbol{B}_{ext}$ is parallel and perpendicular to the simulation system, respectively. In both cases, the wave front reaches the observation point around $\Omega_e t \sim 10$ since it propagates at almost C_v (see Fig. 3). Since a fraction of the pump energy is consumed for the generation of the ES components which accompany the EM propagation prior to the three-wave coupling taking place, the transmission ratio of the EM waves is not 100%. As time elapses, approximately from $\Omega_e t \sim 20$ to 27, the transmission ratio decreases and reaches about 70% of the initial pump energy for the parallel case. The decrease in the pump wave energy is caused by the consumption in the coupling process: the EM wave profile displayed in panel (a) of Fig. 4 shows the decrease of the EM waves which is obviously found in the upper region of the panel (approximately after $\Omega_e t \sim 20$) and spread obliquely along the direction of the EM propagation. As stated earlier, the pump

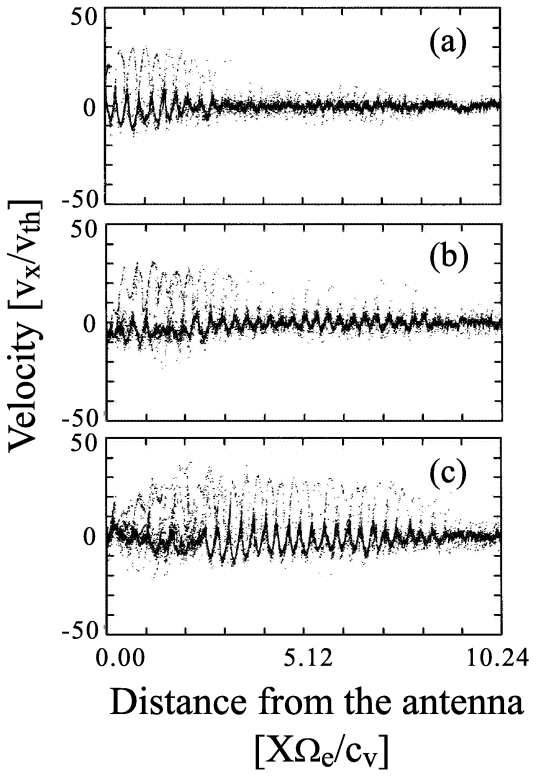

Fig. 7. Phase diagrams of electrons in a plane of V_x versus x at different times: **(a)** $\Omega_e t = 14.08$ **(b)** 16.64, and **(c)** 19.20. The velocity values are normalized to the initial thermal velocity of electrons.

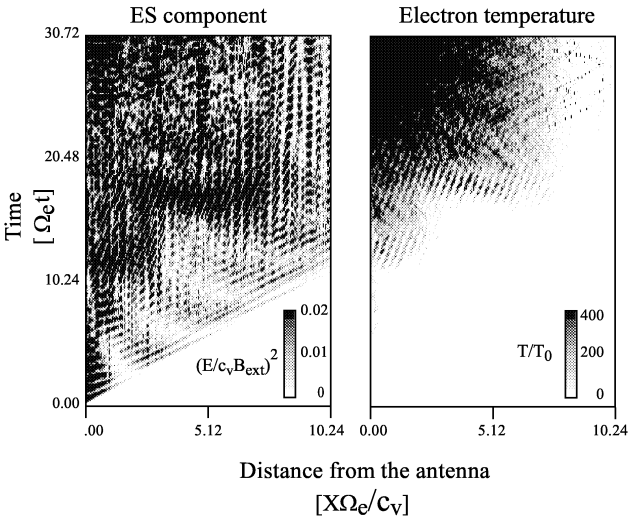

Fig. 8. Excited ES component and associated electron temperature for a case where $\boldsymbol{B}_{ext}$ is along the y direction which is perpendicular to both directions of the pump wave propagation and current oscillation of antenna. The intensity of the pump wave is constant and equal to $E_0/|\boldsymbol{B}_{ext}C_v| = 2.5$.

waves which propagate in the forward direction are weakened at the region where the first ES burst is found around $0.5 < X\Omega_e/C_v < 2.5$ and $12 < \Omega_e t < 16$. Then the weakened pump waves propagate with C_v and reach the end of the simulation system around $22 < \Omega_e t < 26$. Moreover, the second interaction which occurs around $3 < X\Omega_e/C_v < 5$ and $16 < \Omega_e t < 20$ also weakened the pump waves because the first and second interactions occur approximately on the same propagation line, as shown in panel (b) of Fig. 4. This situation causes the large drop of the pump wave energy observed at $\Omega_e t \sim 25$ in panel (a) of Fig. 9.

In the parallel case, the transmission ratio of the pump waves recovers because further three-wave coupling becomes difficult due to the change in the plasma condition by the temperature increase. In the perpendicular case, however, the transmission ratio keeps decreasing and drops down to approximately 20%. This occurs because the coupling continuously occurs, even if the local electrons are heated by the excited ES waves. Eventually a large amount of pump energy is consumed for both the excitation of ES waves and the electron heating in the coupling process in the present model.

4.4 ES enhancement with the speed of light

In Fig. 4, we see an ES component propagating with C_v prior to the three-wave coupling process. The electric field component E_z of the pump wave induces a displacement of electrons in the z direction. The associated V_z, when combined with the wave B_y, induces a displacement in the x direction, which generates an E_x field. Namely, $V_z \times B_y$ causes the E_x component along the simulation system. This second order effect is important only when E_z and B_y are strong. In the parallel mode, this electric field perturbation is supported by the Langmuir waves at the plasma frequency. In the $\omega - k$ diagram shown in Fig. 3, this component is observed at the region where the line of C_v crosses the plasma frequency. When we reduce the intensity of the pump waves, the nonlinear terms becomes weak and the resulting electric field component will disappear.

In the perpendicular case, where $\boldsymbol{B}_{ext}$ is along the y direction, this nonlinear effect is emphasized because $\boldsymbol{B}_{ext}$ is added to the above B_y. In panel (a) of Fig. 8, intense ES components are observed in the vicinity of the antenna.

4.5 Comparison with a real experiment

In a true three-wave coupling experiment in the ionospheric plasma, the pump wave frequency is several GHz, while the local plasma frequency is of the order of MHz. This frequency ratio is more than two orders larger than the one we adopted in the current numerical experiments. For instance, the ratio of the pump wave frequency to the plasma frequency is approximately 3 in the present study, while it is about 400 in an ionospheric plasma. Although not shown here, the growth rate of ES waves excited in the three-wave coupling is inversely proportional to the pump wave frequency. This implies that the growth rate of the ES waves is much reduced in the real experiment. In the present study, ES waves

are strongly excited in a couple of time intervals of the electron gyroperiod which is roughly equal to one μs. Since the growth rate is reduced in the real experiment, the time interval needed for the ES wave excitation can be several hundred μs.

In a situation of a large frequency ratio, we can have a large parallelogram for the three-wave coupling in a $\omega - k$ diagram. In this case, excited low-frequency ES waves have a wavenumber approximately twice as large as the wavenumber of the pump wave. Since the wavelength of the pump wave is approximately 10 cm, the wavelength of the corresponding ES wave can be around 5 cm. Meanwhile, the Debye length in the Low-Earth Orbit (LEO) is several mm, which is much smaller than the wavelength of the above ES waves. This implies that the excited ES waves are less affected by Landau damping.

In a real experiment, ram/wake regions are created by the relative motion of the spacecraft to the ionosphere. In the LEO, ions are responsible for the plasma density variation at the ram/wake regions due to the small thermal velocity. According to the present study, the coupling process itself is not influenced by the ion dynamics. However, it may be possible that the three-wave interaction is affected by the change of the background density which is due to the ion dynamics. Since this analysis is beyond the scope of the present study, we will leave it as future work.

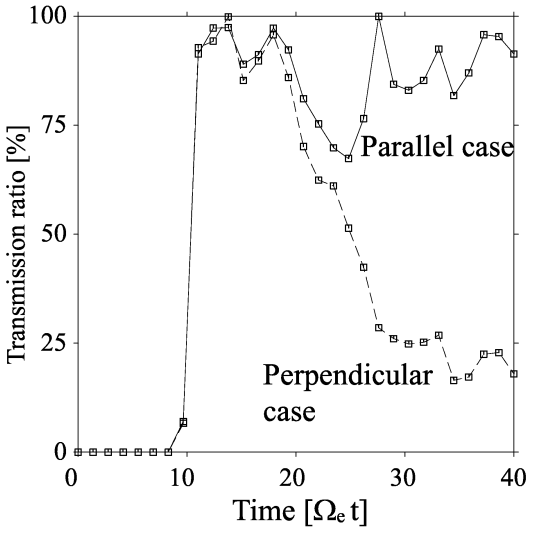

Fig. 9. Pump wave energy detected at the end of the simulation box ($X\Omega_e/C_v$ =10.24) as a function of time. Up to $\Omega_e t = 20$, the two profiles are approximately the same. But in the perpendicular case, the coupling process can continue since the ECH waves propagation characteristics are not very sensitive to the plasma temperature. The transmission of the pump wave is therefore much reduced.

5 Summary

In order to study the nonlinear wave/wave-particle interaction associated with the microwave power transmission (MPT) in space plasmas, we performed one-dimensional simulations with the electromagnetic PIC model. In the present study, we particularly focused on the spatial variation of the coupling process which is difficult to examine theoretically.

In the simulation space filled with magnetized plasma, we continuously emit intense electromagnetic waves from an antenna located at one edge of the simulation system. When the electromagnetic pump waves are intense enough, a three-wave coupling occurs, which is the result of a nonlinear interaction between the forward and backward propagating high-frequency electromagnetic waves and a low-frequency electrostatic wave propagating in the forward direction. The results show that a fraction of the electromagnetic waves emitted from the antenna are backscattered by the background plasma, which induces electrostatic waves at the plasma frequency. In the parallel case, the induced ES waves correspond to the Langmuir mode. The ES waves cause electron heating and the local plasma condition changes. Consequently, the three-wave coupling is weakened and the pump EM wave can propagate through the background plasma with little attenuation. Then the second interaction takes place in a different region. Due to the electron heating again by the excited ES waves, the electron temperature has increased overall so that the plasma condition required for the next three-wave coupling is not satisfied. As a result, the transmission ratio of the pump wave is maintained at around $90-100\%$ in this case. In the perpendicular case, however, the responsible ES wave is a UHR mode of the ECH waves. Since the UHR mode is less sensitive to the electron temperature, the three-wave coupling process continues periodically in time, even if the temperature increases. As a result, electrons are continuously heated and the temperature becomes much more than that of the parallel case. Eventually, approximately 20% of pump energy can propagate through the simulation system because most of the pump energy is consumed in the three-wave coupling process.

As a next step, we need to perform two-dimensional simulations with a model in which microwaves are emitted with an array antenna. By controlling each phase of the array antenna, we can make a focal point of the microwave power at a certain region in the two-dimensional simulation space. By using this model, we will be able to examine the three-wave coupling process in a more realistic situation in terms of the diffusion of the heated electrons and the dependence of the interaction on the angle between the microwave propagation and $\boldsymbol{B}_{ext}$. Preliminary results of such a study will be reported in another paper.

Acknowledgements. We are grateful to Naoki Shinohara for the discussion on the active MPT experiment planned with the exposed facility of the International Space Station.

References

Carlson, Jr., H. C. and Duncan, L. M.: HF excited instabilities in space plasma, Radio Sci., 12, 1001, 1977.

Duncan, L. M. and Behnke, R. A.: Observations of self-focusing electromagnetic waves in the ionosphere, Phys. Rev. Lett., 41, 998, 1978.

Fejer, J. A.: Ionospheric modification and parametric instabilities, Rev. Geophys. Space Phys., 17, 135, 1979.

Glaser, P. E.: Power from the sun: its future, Science, 162, 857, 1968.

Kaya, N., Matsumoto, H., and Akiba, R.: Rocket Experiment METS Microwave Energy Transmission in Space, Space Power, 11, 267, 1993.

Kaya, N., Matsumoto, H., Miyatake, S., Kimura, I., Nagatomo, M., and Obayashi, T.: Nonlinear interaction of strong microwave beam with the ionosphere: MINIX rocket experiment, Space Solar Power Rev., 6, 181, 1986.

Matsumoto, H.: Numerical estimation of SPS microwave impact on ionospheric environment, Acta Astronaut, 9, 493, 1982.

Matsumoto, H., Hashino, Y., Yashiro, H., Shinohara, N., and Omura, Y.: Computer Simulation on Nonlinear Interaction of Intense Microwave with Space Plasmas, Electronics and Communications in Japan, Part3, 78, 89, 1995.

Matsumoto, H. and Kimura, T.: Nonlinear excitation of electron cyclotron waves by monochromatic strong microwave: computer simulation analysis of the MINIX results, Space Solar Power Rev., 6, 187, 1987.

Nishikawa, T.: Computer Experiments on Nonlinear Interactions of Intense Electromagnetic Waves with the Ionospheric Plasma, Master's thesis, Dept. Electrical Eng., Kyoto University, 1999.

Perkins, F. W. and Goldman, M. V.: Self-focusing of radio waves in an underdense ionosphere, J. Geophys. Res., 86, 600, 1980.

Perkins, F. W. and Roble, R. G.: Ionospheric heating by radio waves; predictions for Arecibo and the satellite power station, J. Geophys. Res., 83, 1611, 1978.